

The lattice distortion of nickel particles generated by spark discharge in hydrocarbon dielectric mediums

Yifan Liu¹ · Xianglong Li¹ · Yan Li¹ · Zhankui Zhao¹ · Fushi Bai²

Received: 7 October 2015 / Accepted: 4 February 2016 / Published online: 22 February 2016
© Springer-Verlag Berlin Heidelberg 2016

Abstract Nickel particles were prepared by the ultrasound-aided spark discharge in pure water and hydrocarbons (kerosene and EDM fluid). The element composition and lattice structure were analyzed by EDS and XRD, respectively. The EDS indicated a high-purity powder was generated in pure water. For hydrocarbons, the carbon was detected as the majority impurity dissolved into the Ni interstitial sites, and the quantitative XRD revealed that the peak positions are lower than those of the corresponding perfect Ni crystal. The d-spacing deviation increases with the effect of ultrasound in hydrocarbons, while the distortion is negligible for pure water. We reported the composition, interatomic distances, and distortion of the Ni particles resulting from C doping. These findings revealed a new method to synthesize the solid solution via the spark discharge.

1 Introduction

Spark discharge is widely applied to fabricate the metallic particles due to the simple and low cost of construction and operation of the setup [1, 2]. The spark discharge generated between two submerged liquids or gases has been considered to synthesize particles of different materials in recent years [3–15]. This method can produce particles with a wide range of sizes from a few tens of nm to several tens of

microns, depending on state from which the particles are quenched in the ambient cryogenic mediums [3]. In fact, the morphology and composition are influenced by the cryogenic surrounding like liquid and gas. Three different types of cryogenic mediums were selected in this process including condensed gas (liquid nitrogen), flowing gas, and liquid. Monastyrsky [3] and Solomon [4] obtained mixed metallic powders in liquid argon and liquid nitrogen dielectrics via spark discharge. They investigated the microstructural and chemical characteristics of powders generated with different process conditions. Nguyen and Berkowitz [5] produced high-purity magnetized particles by spark erosion in liquid nitrogen. For the condensed gas, a sealed apparatus should be managed in the generation process. Han [6] and Messing [7] studied to generate the monometallic nanoparticles via the spark discharge with a flowing clean gas. They mainly focused on investigating the explanation of spark parameters and flow pattern on the size distribution and concentration of particles. Plus, in the investigation of Messing [7], the unitary metallic lattice formed an expansion due to the presence of carbon instead of the element of flowing gas. Byeon [8] had investigated on synthesizing binary hollow metallic nanoparticles via a high voltage with a flowing nitrogen. The properties of binary metal were improved by the biocompatibility. Tabrizi [9, 10] used a spark discharge system to synthesize mixed metallic nanoparticles with different flowing gases. He verified the mixed nanoparticles form a continuous solid solution, and crystalline mixed phases were found in all cases. Sahu [11] and Peng [12] generated monometallic Cu and Ni nanoparticles using spark discharge in deionized water, respectively. Sahu [11] used polyvinyl alcohol and polyethylene glycol as stabilizers to prevent agglomeration and coagulation. Peng [12] added silicon element in the generation surrounding to control the size distribution.

✉ Xianglong Li
lixianglong@scu.edu.cn

¹ College of Manufacturing Science and Engineering, Sichuan University, Chengdu 610065, Sichuan, China

² Institute of Dynamics and Vibration Research, University of Hannover, 30167 Hannover, Germany

Actually, the purity of metallic powders was easily affected by the additions. Tseng [13] synthesized Au nanoparticles in ethanol via spark discharge. His experimental results indicated the lattice structure was not changed. Allagui [14] synthesized the Ni and Pt nanoparticles in acidic and alkaline mediums. The results indicated that the compositions of nanoparticles varied with the different process conditions. However, the variation of lattice structure was not investigated in his research. Dvornik [15] used spark erosion to synthesize nanostructured WC–Co particles in distilled water. In his experiments, the results indicated the quenching of Co in the particles promoted the lattice distortion.

In our previous researches [16, 17], we found that hollow Ni particles could be fabricated via the electric discharge machining (EDM) device. We mainly proposed the formation mechanism of the hollow metallic particles and investigated the relationship between size distribution and various system parameters (dielectric mediums, electric parameters). In our investigation, the effect of ultrasound vibration and cavitation has been combined with the EDM to improve the hollow appearance and decrease the size distribution based on the innovation method [18, 19]. For the further research, we verified the element composition and the crystal structure, and we found an unintentional phenomenon that high-pure Ni particles were hardly obtained in the hydrocarbons, and the crystal structure had an obvious expansion comprising the perfect Ni crystal. The hydrocarbons reacted from the spark heat were contributed to the suspension of Ni nanoparticles. Actually, the chemical reaction of hydrocarbons would create some derivatives (supporting in Sect. 3.1) as well as some atoms like carbon and hydrogen. Hence, the effect of impurity on the lattice structure should be investigated. Carbon is commonly present in the iron-group transition metals (Fe, Co, Ni) either as an impurity or as an alloying agent [20]. As the solute in a transition metal, C occupies interstitial

sites due to its relatively small atomic size [21]. Various kinds of binary interstitial solid solution have been synthesized by chemical reaction [22–24]. They mainly discussed the effect of impurities on the key properties of solid solutions based on the first-principles calculation.

In this study, we proposed a reasonable method to generate Ni–C interstitial solid solution with an unintentional C doping. To verify the element composition of the productions and the lattice structures with different dielectric mediums and ultrasound frequencies, a series of experiments were carried out. Then, the samples were observed by DES, and the crystal structure was identified by XRD, respectively. Based on the DES results, the calculated d-spacing and deviation value of three diffraction planes, we explained the reason for the expansion of the lattice structure caused by the C doping and ultrasound.

2 Experimental procedure

Figure 1 shows the schematic diagram of our ultrasound-aided EDM experimental setup developed to produce Ni particles. The system consists of a spark discharge generator and an ultrasound generator. The spark energy is obtained by a numerical control EDM machine E46PM (Jiangsu Excellent Numerical Control Equipment Co., Ltd., Jiangsu, China) with a variable electrical current ranging from 1.5 to 60 A, a variable pulse width ranging from 2 to 1200 μ s, and a variable gap voltage ranging from 30 to 120 V. The servo system controls the tool electrode to maintain an optimal distance in micrometers. The ultrasound oscillators are attached on opposite sides of the stainless steel processing box with a variable ultrasound frequency shifting from 28 to 68 kHz. We conducted the high-purity Ni rods (purity better than 99.9 %, Tianjin Chengshuo Steel Trading Co., Ltd., Tianjin, China) as the tool electrode (cathode) and workpiece electrode (anode). The present investigation was conducted in a laboratory environment with three dielectric mediums including

Fig. 1 Experiment setup used for generating the Ni particles

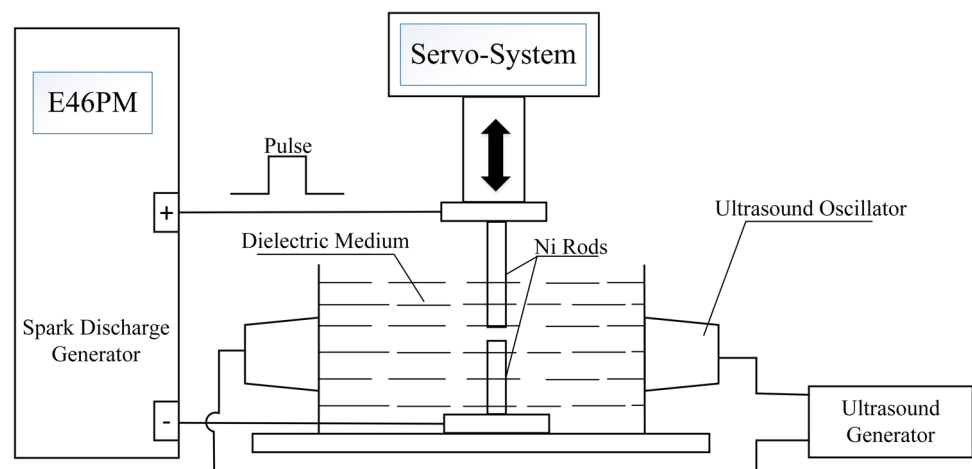


Table 1 The experimental condition of each sample

Sample	1	2	3	4	5	6	7	8	9
Frequency	0	28 kHz	68 kHz	0	28 kHz	68 kHz	0	28 kHz	68 kHz
Dialectic mediums	Kerosene			EDM fluid			Pure water		
Electrical parameters	Current = 15 A, Voltage = 45 V, Plus Width = 300 us								
Time	1 h								

the kerosene, EDM fluid, and pure water. As the hydrocarbons, the kerosene and EDM fluid are regarded as the petroleum-based products. The difference of these two types of hydrocarbons is that the EDM fluid has more percentage of carbon and hydrogen. The flash point of kerosene and EDM fluid ranges at around 100 and 260 °F, respectively. The density of hydrocarbons is varying at different temperatures. Here, the density of kerosene and EDM fluid is 0.780 and 0.770 g/cm³ at room temperature, respectively. For the pure water, the density is 1 g/cm³ at 25 °C. The entire research was carried out with a 15A current, 45 V gap voltage and 300 μs pulse width with a fixed time. The experimental conditions are given in Table 1.

The particles were observed by scanning electron microscope (SEM; Hitachi S-4700; Hitachi Ltd., Japan) to analyze particle surface morphologies. The composition analysis was carried out by energy-dispersive spectroscopy (EDS; JSM-7500F, JEOL, Japan). The crystal structure was identified by X-ray diffraction (XRD; X'Pert Pro MPD, Philips, Netherlands). The X-ray spectrum was analyzed based on the standards presented by the Joint Committee on Powder Diffraction Standards (JCPDS, data file PDF #65-0380).

3 Results and discussion

3.1 The EDS analyses of particles produced in three dielectric mediums

The EDS spectrum was performed to determine the material composition of the particles with different dielectric mediums to confirm the purification of crystallization process. The analysis results of particles generated in the kerosene, EDM fluid and pure water without ultrasound are shown in Fig. 2a–c, respectively.

All the figures show that the samples mainly contained three elements including carbon(C), oxygen (O), and nickel (Ni). The results are given in Table 2.

For the kerosene, the proportions of three elements are 3.83, 1.76, and 94.41 %, respectively. For the EDM fluid, the proportions are 2.93, 1.10, and 95.97 %, respectively. As the petroleum-based products, the kerosene and EDM fluid consist of complex mixtures of aliphatic, aromatic, and polycyclic aromatic hydrocarbons. Hence, the presence of C in the sample is due to the decomposition of hydrocarbons in a high temperature. The decomposition has an

endothermic reaction to break the C–H bond to generate carbon and hydrogen. The thermal decomposition of hydrocarbons can be represented by the simplified next reaction [25]:



The source of oxygen could come from the dissolved air in the dielectric media or occluded air caused by filling the box with hydrocarbons in an open processing environment. For the pure water, the proportions of the three elements are 0.38, 1.76, and 97.84 %, respectively. It is known that the pure water does not contain a C element. Hence, the resource of 0.38 % C is produced by the conductive tape which is used as the fixer to analyze the sample. In addition, the particles could be coated or adhered with a C element which was left in the box in the last kerosene or EDM fluid experiment. The proportions of oxygen are almost invariable in different dielectric mediums. The proportion of carbon in the particles generated in the hydrocarbons is about ten times than in the pure water. The proportion of Ni in pure water is near 98 %, and the particles produced in the water had a higher purity than the kerosene and EDM fluid. The impurity doping would cause crystalline distortion which is discussed in Sect. 3.2.

3.2 The structure analysis of particles produced in three dielectric mediums without ultrasound

The structures of the products fabricated by spark discharge under different dielectric mediums were identified by XRD. The scanning range was from 15° to 90° using Cu Kα ($\lambda = 1.54056 \text{ \AA}$) and operated at 40 kV and 200 mA. The step size of 0.02° and scan rate of 5° per min were used for recording the XRD spectra of samples. Structure refinement was performed using MDI JADE 5.0 software, which can perform powder diffraction data analysis and acquisition.

Figure 3a shows the XRD spectrum of the Ni micron particles generated by spark discharge in the hydrocarbon dielectric mediums (kerosene and EDM fluid). Figure 3b shows the spectrum of the Ni particles generated in the pure water. The XRD data indicated that the spark-generated Ni particles in different dielectric mediums were face-centered cubic (FCC) crystallites. The peak patterns and

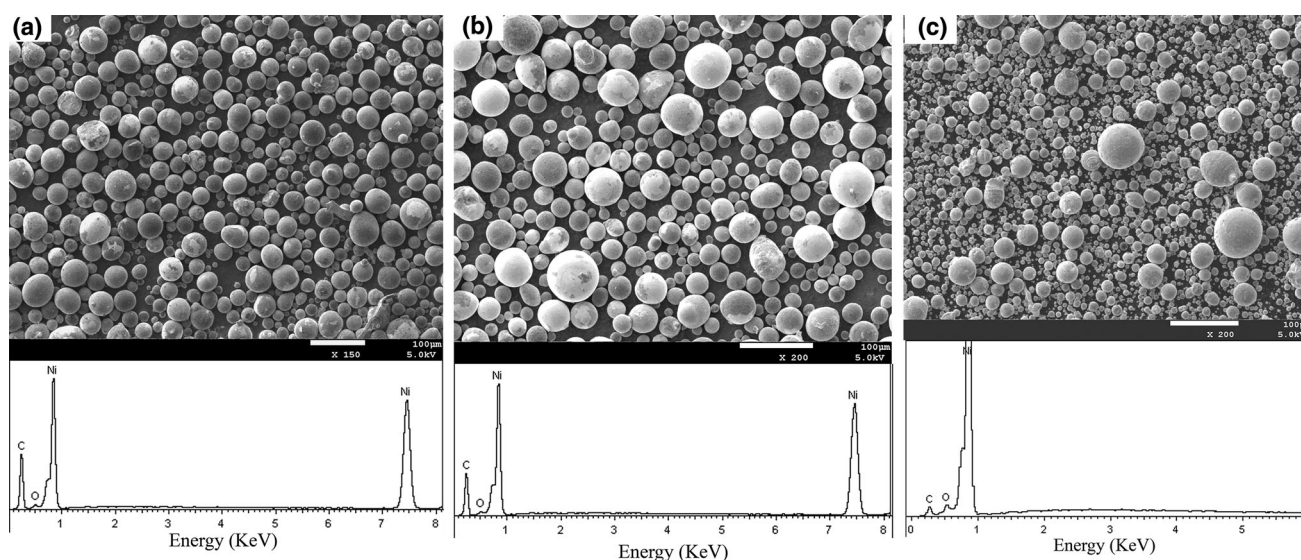


Fig. 2 The SEM-EDS analysis of particles generated in the hydrocarbons and pure water

Table 2 The EDS analysis datasheet of Ni particles in different dielectric mediums

Elements	Mass (%)			Atomic (%)		
	Pure water	Kerosene	EDM fluid	Pure water	Kerosene	EDM fluid
C	0.38	3.83	2.93	1.74	15.64	12.52
O	1.78	1.76	1.10	6.15	5.40	3.53
Ni	97.84	94.41	95.97	92.11	78.96	83.95
Totals	100	100	100	–	–	–

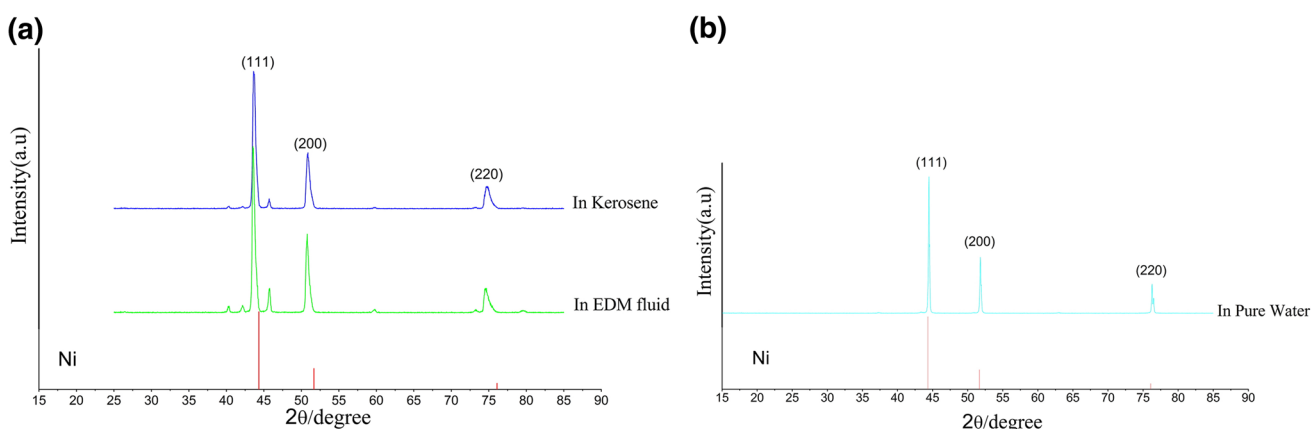


Fig. 3 XRD patterns of Ni particles generated in different dielectric mediums: **a** in hydrocarbons (*blue* for kerosene and *green* for EDM fluid) and **b** in pure water (*cyan*). *Red bars* correspond to JCPDS 65-0380

peak positions for all diffraction patterns closely match those for perfect FCC Ni (JCPDS, data file PDF #65-0380). Three characteristic peaks for Ni in different dielectric mediums were observed and marked by the (111), (200), and (220) planes.

Figure 3 shows XRD patterns of Ni particles generated in different dielectric mediums: (a) in hydrocarbons (blue

for kerosene and green for EDM fluid) and (b) in pure water (cyan). Red bars correspond to JCPDS 65-0380.

For the sample generated in pure water, the XRD pattern revealed the formation of the desired Ni monometallic particles with a higher purity (98 %, referencing information Table 2). The XRD patterns did not show any other additional peaks, indicating that a simple monometallic

particle had been formed. We had not observed any detectable impurity peaks related to Ni or its oxides. Absence of impurity peaks indicated that the hydrogen or oxygen did not exist in the lattice sites of Ni. We assumed that all the impure elements are not entering inside and few numbers (1.78 % oxygen) are adhering to the surface; the intensity of their diffraction peaks is so negligible that the peaks could not be detected in the XRD pattern.

For the samples generated in hydrocarbons, the XRD pattern illustrated the formation of the particles with a particular impurity. The significant features in the XRD of the samples were the reduction in peak intensity and the appearance of the diffuse peak around the diffraction peak. The peak positions were somewhat shifted to lower angles for the particles generated in hydrocarbons. This shift indicated a small change in lattice parameter and was relevant to the doping of the detected impure element. The doping impurity increased the full width at half maximum (FWHM) shown in Fig. 3.

3.3 The distortion of lattice with an impurity doping in the hydrocarbons

In the spark situ, spark plasma will produce mixed species from nickel and dielectric medium, namely Ni atoms and clusters, Ni aggregations and droplets, atoms and some carbon which came from the decomposition of hydrocarbons.

Reflections (111), (200), and (220) were used to determine the lattice parameters. The standard diffraction angles of the (111), (200), and (220) planes for the perfect Ni crystal are $2\theta = 44.35^\circ$, 51.67° , and 76.10° , respectively. The corresponding interplanar spacing is $d_{hkl}^0 = 2.0409$, 1.7675, and 1.2498 (Å), respectively. The d-spacing of (111) (200), and (220) planes is also calculated based on the peak positions.

We used $\Delta d_{hkl} = (d_{hkl} - d_{hkl}^0)$ to represent the deviation of the generated Ni particles from the idea value. Δd_{111} , Δd_{200} , and Δd_{220} were the deviations calculated from the corresponding diffraction planes, respectively. Table 3 lists the measured d-spacing and the deviation of (111), (200), and (220) diffraction planes for the samples 1, 4, and 7, which is established and calculated from the full-pattern Rietveld refinements of the XRD patterns.

The lattice constant of the generated Ni samples was determined from the peak positions using the Bragg's law [26]:

$$2d \sin \theta_{hkl} = \lambda \quad (2)$$

Here, d is the interplanar spacing, θ_{hkl} is the diffraction angle of the (hkl) diffraction plane, and λ is the X-ray wavelength.

The diffraction angle is negatively correlating with the d-spacing as we obtain from Eq. 2. Figure 4 shows a plot of Δd versus the diffraction planes to illustrate the distortion of lattice with the different experimental conditions. The data in Table 3 and Fig. 4 therefore indicated that the diffraction angles of the (111), (200), and (220) of the generated Ni samples deviated significantly from the ideal values of the perfect Ni crystal lattice, while solute atoms were introduced into the Ni particles during the condensation occurred around the electrodes. In the case of pure water (blue line), the nuanced d-spacing offsets (less 0.0056 Å) were negative values which meant the lattice took a nuanced contraction compared with the perfect FCC Ni crystal, and this contraction could be neglected to identify the lattice of sample 7 that did not have a change.

Obviously, the distortion of lattice had an increase in these samples generated in hydrocarbons than the perfect Ni crystal. The value of lattice distortion in hydrocarbons was one order of magnitude higher than in pure water. The d-spacing offsets reached the range of 0.02–0.035 Å for samples 1 and 4. Anyway, the distortion value of (111) plane was highest in these three conditions. The lattice took a distinct expansion compared with the perfect FCC Ni crystal, and this expansion was caused by the carbon doping. This doping denoted that a solid solute (like C) dissolves in a solid solvent (like Ni) to be a solid solution. This solution does not destroy the crystalline structure of the parent phase. Matsui [20] investigated the enthalpies of solution for carbon doping in the FCC Ni. He proposed that the solution enthalpy of the Ni–C octahedral interstitial solid solution was lower than the substitutional and tetrahedral-interstitial solid solutions, and the carbon atoms preferred octahedral interstitial sites. Besides, the metalloid atoms move at random into the transition metal and occupy the interstitial sites due to its relatively small atomic size.

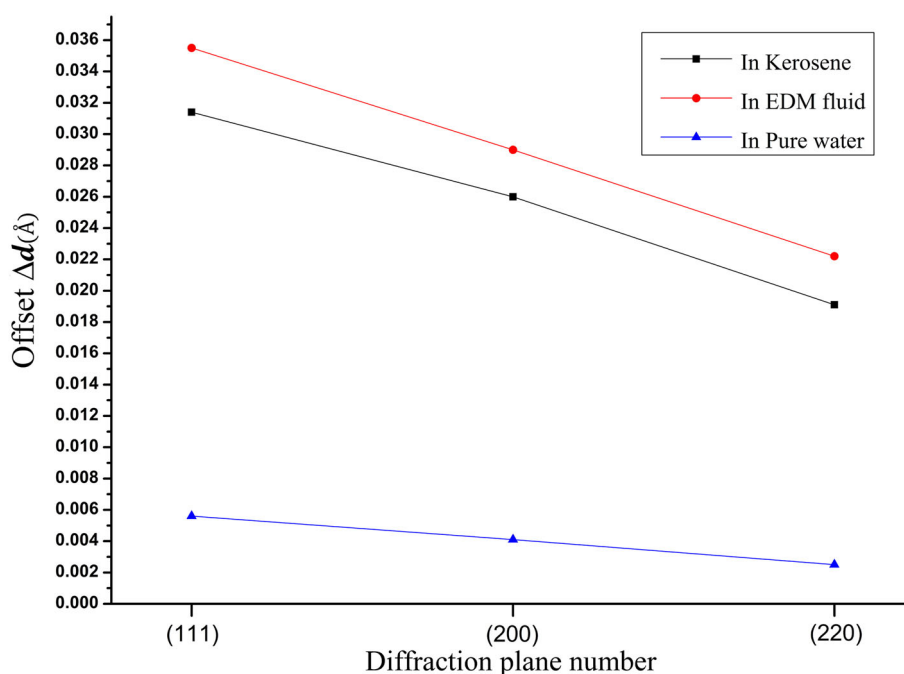
3.4 The structure analysis of particles produced in three dielectric mediums with ultrasound

It is worth noting that previous studies [16, 17] on the formation mechanism of the hollow particles have revealed the effect of ultrasound on the size or morphology of the

Table 3 The calculated d-spacing and deviation of (111), (200), and (220) diffraction planes with different dielectric mediums

d-spacing/ Δd_{hkl}	1	4	7
d_{111} (Å)/ Δd_{111} (Å)	2.0723/0.0314	2.0764/0.0355	2.0353/−0.0056
d_{200} (Å)/ Δd_{200} (Å)	1.7935/0.0260	1.7965/0.0290	1.7634/−0.0041
d_{220} (Å)/ Δd_{220} (Å)	1.2689/0.0191	1.2720/0.0222	1.2473/−0.0025

Fig. 4 The distortion of lattice for three diffraction planes in different dielectric mediums



particles. In the literature, the reported experiments showed significant variation in the size distribution. In the three dielectric mediums, the amount of less than 5 μm particles generated with ultrasound is higher than the productions generated without ultrasound. It is necessary to investigate the effect of ultrasound on the crystal structure of particles.

Figure 5 shows the XRD spectrum of the Ni micron particles generated in the hydrocarbon dielectric mediums (left) and pure water (right) with the assist of ultrasound, and the performed ultrasound frequency was 28 kHz (up) and 68 kHz (down). For the figure, it could be found that three characteristic peaks for Ni in different dielectric mediums with different ultrasound frequencies had a similar trend when compared to the Ni particles generated without ultrasound. The XRD data indicated the ultrasound wave did not destroy the crystalline structure (FCC) of the parent phase. The peak intensity and height reduced with increasing ultrasound frequency for the samples generated in hydrocarbons as well as in pure water. The FWHM of (111), (200), and (220) peaks for samples generated in hydrocarbons with ultrasound were larger than those of samples generated in pure water. In the case of samples 8 and 9, the increase in the FWHM of three peaks meant that the crystallinity could be affected by the ultrasound vibration. Compared with the sample 7, the crystallinity of particles without ultrasound was higher than those two samples. For the samples generated in hydrocarbons, the crystallinity involved in ultrasound was lower than the samples generated without ultrasound. This degradation of crystallinity was originated from the ultrasound wave and

intragranular impurities. The peak positions were still shifted to lower angles for the particles generated in hydrocarbons, while increasing ultrasound frequency was added in the generation process. We proposed that the ultrasound was contributed to this offset and was in favor of driving some impure elements to implant into the octahedral interstitial sites. Hence, the solid solution behavior was still observed in these samples. In this investigation, we revealed that C doping in the FCC Ni particles increased as a function of ultrasound frequency in next section.

3.5 The effect of ultrasound on the lattice spacing and interstitial carbon doping

Table 4 lists the calculated deviation of (111), (200), and (220) diffraction planes for the samples generated in three dielectric mediums with different ultrasound frequencies. The relationship between the lattice distortion of the particles and the ultrasound frequency is shown in Fig. 6.

Figure 6a shows a plot of Δd versus the diffraction planes to illustrate the distortion of lattice in pure water with different ultrasound frequencies. The distortion was scarcely changing (less 0.002 \AA), while the ultrasound frequency raised to 68 kHz. While the frequency was 28 kHz, the distortion trend was similar to the sample generated without ultrasound. Compared to these three straight lines, the nuanced d -spacing offsets (less 0.006 \AA) were negative. We deduced that a high frequency does not promote the expansion or contraction behavior when the

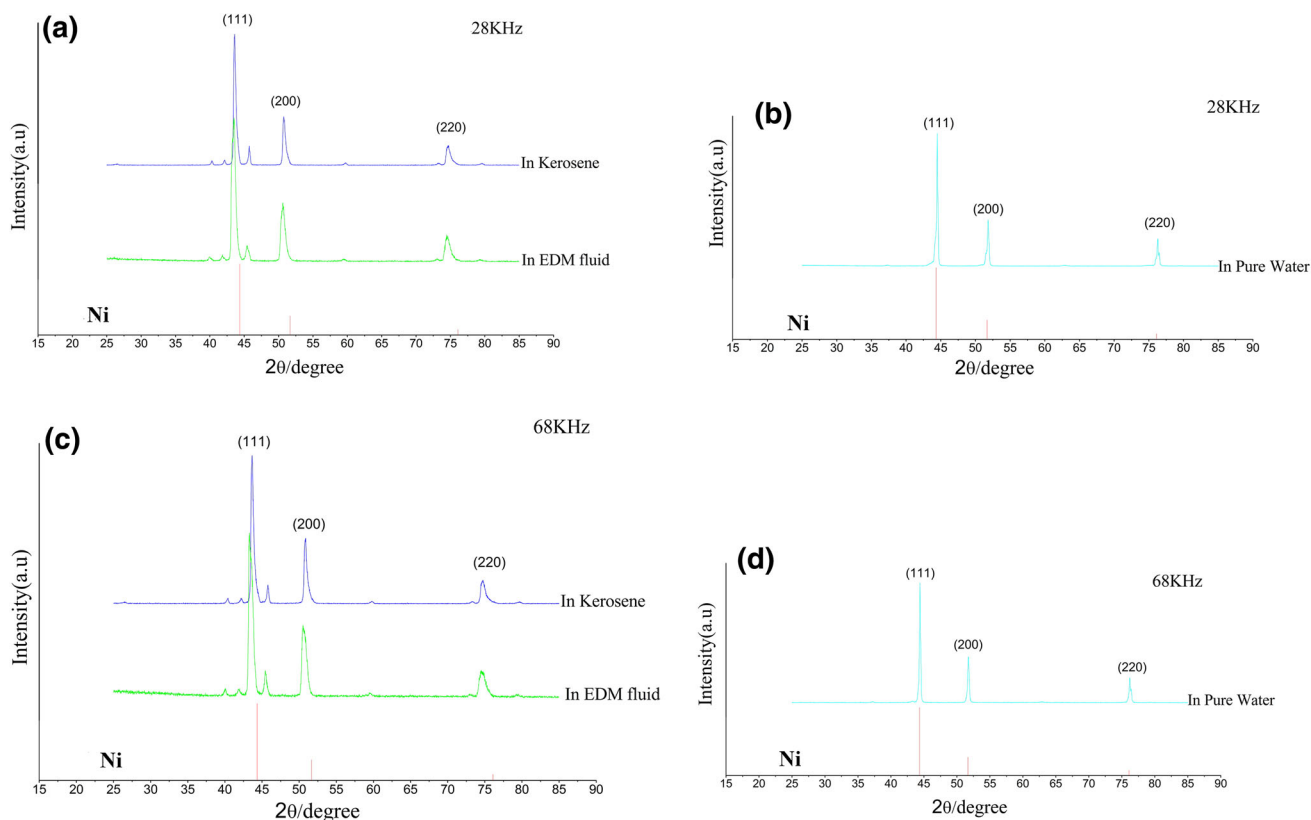


Fig. 5 XRD patterns of Ni particles generated in different dielectric mediums by the ultrasound-aided spark discharge process: **a** and **c** in hydrocarbons with 28 and 68 kHz, respectively; **b** and **d** in pure water with 28 and 68 kHz, respectively

Table 4 The calculated deviation of (111), (200), and (220) diffraction planes with different dielectric mediums and frequencies

Δd_{hkl}	2	3	5	6	8	9
Δd_{111} (Å)	0.0333	0.0314	0.0378	0.0460	-0.0057	-0.0022
Δd_{200} (Å)	0.0309	0.0264	0.0343	0.0383	-0.0047	-0.0015
Δd_{220} (Å)	0.0216	0.0204	0.0218	0.0230	-0.0025	-0.0012

molten or gasified Ni atom clusters aggregate and solidify the particles in the pure water. Hence, the expansion of Ni sample with 28 kHz is lower than the corresponding perfect Ni crystal. The ultrasound made no difference on the distortion of lattice although the generation surrounding was full with some impurity elements like hydrogen and oxygen. This demonstrated the hydrogen and oxygen were

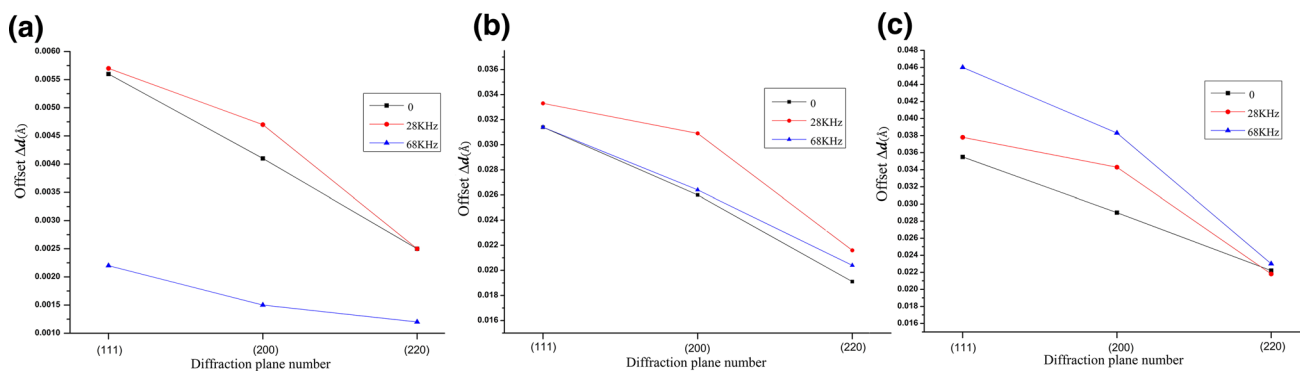


Fig. 6 The distortion of lattice for three diffraction planes in different dielectric mediums with different ultrasound frequencies: **a** in water with 0, 28, and 68 kHz; **b** in kerosene with 0, 28, and 68 kHz; **c** in EDM fluid with 0, 28, and 68 kHz

hardly doped in the Ni. In the other words, the solid solution was hardly formed in the pure water with or without ultrasound.

Figure 6b, c illustrates the lattice expansion value in the kerosene and the EDM fluid with different ultrasound frequencies, respectively. In the kerosene, while the frequency was 68 kHz, the distortion trend was similar to the sample generated without ultrasound. While the frequency was 28 kHz, the expansion value was more than 68 kHz. In the EDM fluid, the results were opposite to the kerosene for the 28 and 68 kHz. The expansion was obvious with a high frequency (68 kHz). Plus, the expansion value of each plane for EDM fluid was almost more than kerosene. Compared to the straight lines for different conditions, the expansion value of samples generated in hydrocarbons with ultrasound was more than without ultrasound. We concluded that the expansion behavior was promoted after the ultrasound was introduced into the process. However, the effect of ultrasound was not reflected on the crystallization nature for the Ni, which was verified in Fig. 6a. The ultrasound was mainly contributed to the formation of solid solution. Therefore, we believed that the ultrasound vibration plays an important role on enhancing the ability of doping impurity elements into the octahedral interstitial sites.

4 Conclusion

The electrical discharge machining aided by ultrasound method in a liquid environment is a simple, effective technique to generate particles. We reported the structural attributes like interatomic distances, distortion, and composition of the Ni particles resulting from the C doping. The EDS studies indicated a high purity (98 %) of nickel particles generated in pure water. The particles are hardly oxidized by the oxygen decomposed by the high temperature. Quantitative XRD analysis on the particles generated in pure water demonstrated that the lattice structure did not distort under various ultrasound frequencies. The expansion or contraction behavior was not apparent yet in these samples. The EDS results showed an impure degree for these particles generated in hydrocarbons (kerosene and EDM fluid). Even with carbon content as high as several percent, the crystalline FCC Ni lattice is not significantly disrupted. Plus, the XRD analysis demonstrated that the crystal structure of the Ni particles deviates significantly from an increment of the d-spacing deviation (Δd). While the ultrasound was introduced into the generation process, this deviation becomes more obvious from the perfect Ni crystal, which is manifested by an expanded crystal structure. The lattice expansion can be qualitatively

explained in terms of carbon atoms doped and dissolved into octahedral interstitial sites as a result of forming the interstitial solid solution. This carbon doping increases as a function of ultrasound frequency and the type of the dielectric mediums. However, the ultrasound was contributed to enhance the doping process, instead of the crystallization process.

Based on these results, further research should be focused on the following topics. First, the solubility and diffusion of C in Ni should be investigated. Secondly, the mechanical properties of these solid solution particles should be researched.

Plus, the results of this study suggest that the spark discharge can be used to synthesize the solid solution in some hydrocarbons or impure solutions instead of the chemical process.

Acknowledgments This work has been supported by the National Natural Science Foundation, China (Grant Nos. 51275324 and 51435011) and Innovation Method Fund of China (2013IM030500).

References

1. T.V. Pfeiffer, J. Feng, A. Schmidt-Ott, New developments in spark production of nanoparticles. *Adv. Powder Technol.* **25**, 56–70 (2014)
2. B.O. Mueller, M.E. Messing, D.L.J. Engberg, A.M. Jansson, L.I.M. Johansson, S.M. Norlén, N. Tureson, K. Deppert, Review of spark discharge generators for production of nanoparticle aerosols. *Aerosol Sci. Technol.* **46**, 1256–1270 (2012)
3. G. Monastyrsky, P. Ochin, G.Y. Wang, V. Kolomytsev, Y. Koval, V. Tinkov, A. Shcherba, S. Zaharchenko, Structure and composition of titanium spark erosion powder obtained in liquid nitrogen. *Chem. Met. Alloys* **4**, 126–142 (2011)
4. V.C. Solomon, J. Hong, Y.J. Tang, A.E. Berkowitz, D.J. Smith, Electron microscopy investigation of spark-eroded Ni–Mn–Ga ferromagnetic shape-memory alloy particles. *Scripta Mater.* **56**, 593–596 (2007)
5. P.K. Nguyen, S. Jin, A.E. Berkowitz, MnBi particles with high energy density made by spark erosion. *J. Appl. Phys.* **115**, 17A756 (2014)
6. K. Han, W. Kim, J. Yu, J.H. Lee, H. Lee, C.G. Woo, M. Choi, A study of pin-to-plate type spark discharge generator for producing unagglomerated nanoaerosols. *J. Aerosol Sci.* **52**, 80–88 (2012)
7. M.E. Messing, R. Westerstrom, B.O. Mueller, S. Blomberg, J. Gustafson, J.N. Andersen, E. Lundgren, R. van Rijn, O. Balmes, H. Bluhm, K. Deppert, Generation of Pd model catalyst nanoparticles by spark discharge. *J. Phys. Chem. C* **114**, 9257–9263 (2010)
8. J.H. Byeon, Y.W. Kim, Ambient plasma synthesis of Si-Fe hollow nanoparticles and their biocompatibility and lithium storage capacity. *Adv. Mater. Interfaces* **1**, 1300134 (2014)
9. N.S. Tabrizi, Q. Xu, N.M. van der Pers, A. Schmidt-Ott, Generation of mixed metallic nanoparticles from immiscible metals by spark discharge. *J. Nanopart. Res.* **12**, 247–259 (2010)
10. N.S. Tabrizi, Q. Xu, N.M. van der Pers, U. Lafont, A. Schmidt-Ott, Synthesis of mixed metallic nanoparticles by spark discharge. *J. Nanoparticle Res.* **11**, 1209–1218 (2009)
11. R.K. Sahu, S.S. Hiremath, P.V. Manivannan, M. Singaperumal, Generation and characterization of copper nanoparticles using

- micro-electrical discharge machining. *Mater. Manuf. Processes* **29**, 477–486 (2014)
12. H.B. Peng, D.P. Yu, X. Zhang, S.L. Wang, Y.H. Wen, Fabrication of hollow nickel micro-spheres with high degree of hollowness by silicon powder-mixed spark erosion. *Int. J. Mach. Tool Manuf.* **85**, 131–134 (2014)
 13. K.H. Tseng, J.C. Huang, Pulsed spark-discharge assisted synthesis of colloidal gold nanoparticles in ethanol. *J. Nanoparticle Res.* **13**, 2963–2972 (2011)
 14. A. Allagui, E.A. Baranova, R. Wüthrich, Synthesis of Ni and Pt nanomaterials by cathodic contact glow discharge electrolysis in acidic and alkaline media. *Electrochim. Acta* **93**, 137–142 (2013)
 15. M.I. Dvornik, Nanostructured WC–Co particles produced by carbonization of spark eroded powder: synthesis and characterization. *Int. J. Refract. Met. Hard Mater.* **28**, 523–528 (2010)
 16. Y. Liu, X. Li, Y. Wang, F.S. Bai, J. Chen, Effect of system parameters on the size distributions of hollow nickel microspheres produced by an ultrasound-aided electrical discharge machining process. *Particuology* **17**, 36–41 (2014)
 17. Y.T. Wang, X.L. Li, Y.F. Liu, Y. Li, W. Zhao, W.Q. Li, Effect of non-electrical parameters on the size of nickel microspheres produced by an ultrasound-aided electrical discharge machining. *Chin. J. Mech. Eng.* **51**, 195–200 (2015)
 18. L. Hu, Y. Li, X. Li, W. Li, Y. Wan, Study of preparation methods of nanometer-sized hollow nickel spheres based on substance-field model. *Chin. J. Eng. Des.* **20**, 180–184 (2013)
 19. Y. Li, J. Wang, X.L. Li, W. Zhao, Design creativity in product innovation. *Int. J. Adv. Manuf. Technol.* **33**, 213–222 (2007)
 20. C.A. Wert, Precipitation from solid solutions of C and N in α -iron. *J. Appl. Phys.* **20**, 943–949 (1949)
 21. H. Numakura, K. Kashiwazaki, H. Yokoyama, M. Koiwa, An elastic relaxation due to interstitial solute atoms in face-centered cubic metals. *J. Alloys Compd.* **310**, 344–350 (2000)
 22. I. Matsui, T. Uesugi, Y. Takigawa, K. Higashi, Effect of interstitial carbon on the mechanical properties of electrodeposited bulk nanocrystalline Ni. *Acta Mater.* **61**, 3360–3369 (2013)
 23. D.J. Siegel, J.C. Hamilton, First-principles study of the solubility, diffusion, and clustering of C in Ni. *Phys. Rev. B Condens. Matter* **68**, 094105 (2003)
 24. C.A. Schuh, T.G. Nieh, H. Iwasaki, The effect of solid solution W additions on the mechanical properties of nanocrystalline Ni. *Acta Mater.* **51**, 431–443 (2003)
 25. S. Ahmed, A. Aitani, F. Rahman, A. Al-Dawood, F. Al-Muhaish, Decomposition of hydrocarbons to hydrogen and carbon. *Appl. Catal. A* **359**, 1–24 (2009)
 26. X.D. Liu, H.Y. Bang, K. Lu, Z.Q. Hu, The lattice expansion in nanometre-sized Ni polycrystals. *J. Phys. Condens. Matter* **6**, 497–502 (1994)